Proceedings of the Canadian Society for Mechanical Engineering International Congress
32nd Annual Conference of the Computational Fluid Dynamics Society of Canada
Canadian Society of Rheology Symposium
CSME-CFDSC-CSR 2025
May 25–28, 2025, Montréal, Québec, Canada

EFFECT OF PARTIAL SHELTERING ON SPANWISE WAKE INTERFERENCE OF UNEQUAL-HEIGHT TANDEM CIRCULAR CYLINDERS

Ashim Chhetri[1*], Keziah N.D. Hammond[1], Joseph K. Kodie-Ampaw[1], Adime K. Bonsi[1], Ebenezer E. Essel[1]
[1]Department of Mechanical, Industrial and Aerospace Engineering, Concordia University, Montreal, Canada
*ashim.chhetri@mail.concordia.ca

Abstract—Time-resolved particle image velocimetry is used to investigate the effects of partial sheltering on the unsteady wake dynamics of unequal-height tandem cylinders submerged in a turbulent boundary layer (TBL). The height ratio of the cylinders was kept constant at $h/H = 0.75$ based on the aspect ratios of $h/d = 5.3$ for the upstream (UC) and $H/d = 7.0$ for the downstream (DC) cylinders, where h and H represent the height of the UC and DC, respectively and d the diameter of the cylinders. The center-to-center spacing between the cylinders was $4d$, Reynolds number based on the cylinder diameter (d) was 5540 and the submergence ratio was $\delta/H = 1.2$, where δ is the TBL thickness. Measurements were performed in three streamwise-spanwise planes along the height of the tandem cylinders (TC) and single cylinder (SC) identical to the DC. The results showed that wake interference by the DC enhanced the near wall reverse flow region, while reducing the vortex shedding frequency behind the UC compared to the SC. For the DC, the enhanced flow entrainment from the side accelerated the vortex formation of larger structures in the sheltered region, while delaying the vortex formation at the unsheltered free end. As a result, the reverse flow region was reduced in the sheltered portion but enhanced near the free end of the DC.

Keywords; finite wall-mounted cylinders, wakes, vortex shedding, flow-structure interactions

I. INTRODUCTION

Flow around finite wall-mounted cylinders (FWMCs) is encountered in a wide range of engineering applications, including buildings, wind turbines, chimney stacks, cooling towers and offshore structures. Flow past FWMC is characterized by von Karman vortex shedding, tip and base vortices that interact with the regular vortex shedding to form a complex vortex system. The vortex shedding modes are further complicated when two cylinders are arranged in tandem, where the direct interaction of approach flow with the downstream cylinder (DC) is shielded by the upstream cylinder (UC). The resulting wake interference and sheltering of DC lead to vortex-induced vibrations and fatigue failure. Sheltering can also be used as flow control strategy to minimize unsteady loading on high-rise building, reduce pollutant dispersion and drag reduction [1].

The wake structure of single cylinder (SC) depends on the Reynolds number ($Re = U_\infty d/v$) [2], aspect ratio ($AR = H/d$) [3], [4] and submergence ratio (δ/H) [5], where H and d are the height and diameter of the cylinder, and v is the kinematic viscosity of the fluid. The Reynolds number influences the flow separation along the span of the cylinder and is classified into four regimes: subcritical regime ($4 \times 10^2 < Re < 10^5$) characterized by laminar separation, critical regime ($10^5 < Re < 3 \times 10^5$) with laminar-to-turbulent transition, supercritical regime ($3 \times 10^5 < Re < 2 \times 10^6$) and transcritical regime ($Re > 2 \times 10^6$) regimes characterized by fully turbulent separation [2]. The aspect ratio is often used to categorize the flow into two regimes: dipole and quadrupole. However, the interplay between the effects of aspect ratio and the submergence ratio has led to inconsistent critical aspect ratios reported in previous studies [6]. In general, a dipole structure, which is associated with SCs with aspect ratios below the critical value, have a pair of tip vortices that induce a strong downwash flow from the free end of the cylinder [4], [7]. SCs with large aspect ratios exhibit a quadrupole wake structure, characterized by the presence of both pairs of tip and base vortices [5], [8] as shown by Fig. 1a.

For tandem FWMCs the wake interference is influenced by the spacing ratio (s/d), the aspect ratio of each cylinder, and the height ratio between the cylinders (h/H), where s is the center-to-center spacing distance, h represents the height of the UC, and H represents the height of the DC for simplicity (Fig. 1*b*). Based on spacing ratio, the flow structure of identical tandem cylinder ($h/H = 1$) is often categorized into three main regimes: extended body regime ($s/d \leq 2$), reattachment regime ($s/d \in [2,5]$) and co-shedding regime ($s/d \geq 5$) [2], [8], [9]. Unequal-height tandem cylinders ($h/H < 1$) exhibit a more complex topology compared to identical height cylinder due to the impact of partial sheltering of the DC by UC.

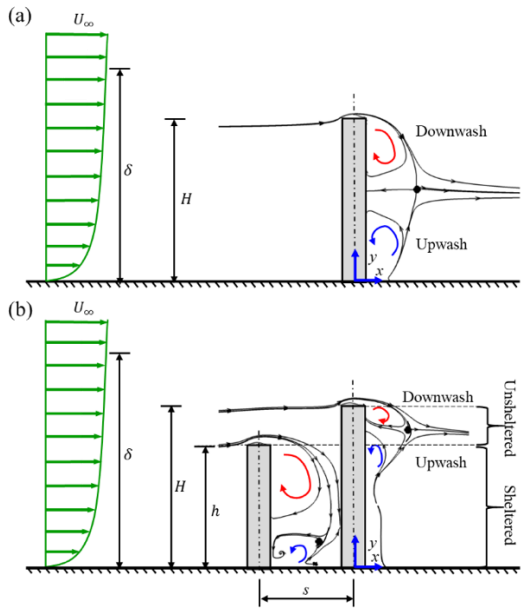

Figure 1. Schematic of the time-averaged flow characteristics for (a) single finite wall-mounted cylinders (FWMC) and (b) unequal-height tandem FWMC.

Despite their prevalence in various engineering applications such as cluster of low and high-rise buildings, the understanding of the unequal-height tandem cylinders is limited.

Hamed et al. [1] used a particle image velocimetry (PIV) to study the effects of height ratio ($h/H = 0.50, 0.75$ and 1.0) and spacing ratio ($s/d = 2, 4$ and 6) on the wake interference of low aspect ratio cylinders ($H/d = 2.5$), and found that the degree of sheltering increases with increasing height ratio and decreasing spacing ratio. Essel et al. [10] experimentally investigated the sheltering effect on a high aspect ratio DC ($H/d = 7.0$) by varying the height ratio ($h/H = 0.10, 0.25, 0.50, 0.75$ and 1.00) at fixed spacing ratio ($s/d = 4$) and found a significant enhancement in degree of sheltering with modified vortex shedding of the DC, as the height ratio increased, compared to an isolated single cylinder. Ouedraogo & Essel [11] showed that decreasing the spacing ratio at a fixed height ratio ($h/H = 0.75$) significantly enhanced the degree of sheltering.

This paper investigates the effects of partial sheltering on the spanwise wake dynamics of unequal-height tandem FWMCs submerged in a TBL ($\delta/H = 1.2$). Detailed measurements were conducted in three streamwise-spanwise planes along the span of a TC with a fixed spacing ratio, $s/d = 4$, and height ratio, $h/H = 0.75$, and a reference SC with aspect ratio of $AR = 7.0$, similar to that of the DC of the TC. The spacing ratio was selected to induce strong wake interference, while the height ratio provided 25% of unsheltered free end of the DC.

II. EXPERIMENTAL SETUP & PROCEDURE

An open recirculating water channel facility equipped with a time-resolved particle image velocimetry (TR-PIV) system at the University of Manitoba was used for the experiments. A 30 −kW variable-speed drive pump moved the flow through a flow conditioning unit before it entered the test section made

Identify applicable sponsor/s here. *(sponsors)*

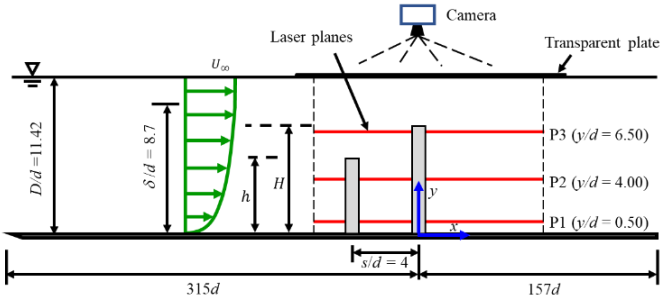

Figure 2. Schematic of experimental setup and nomenclature used in the present study. The PIV measurements were carried out in the horizontal plane (x-z planes) positioned at P1, P2 and P3.

of a transparent acrylic plate. The test section has a dimension of 6.00 m $\times$ 0.45 m $\times$ 0.60 m in the streamwise, wall-normal and spanwise directions, respectively. Fig. 2 shows a schematic of the experimental setup for the two unequal-height cylinders arranged in tandem. Each cylinder was a smooth round acrylic rod of diameter, $d = 12.7$ mm, and was vertically mounted on a flat acrylic false plate lining the entire floor of the test section. The origin of the left-handed Cartesian coordinate system is positioned at the center of the downstream cylinder on the bottom wall. The aspect ratios of the cylinders were fixed at $h/d = 5.3$ for the UC and $H/d = 7.0$ for the DC to achieve a height ratio of $h/H = 0.75$ while maintaining a fixed spacing ratio of $s/d = 4$. The submergence ratio was $\delta/H = 1.2$ while the Reynolds number ($Re = U_\infty d/\nu$) was 5540. Additionally, experiments were performed for a single cylinder (SC) identical to the DC as a reference test case.

The planar TR-PIV system was used to measure the velocity fields. The flow was seeded with $10\ \mu m$ silver-coated hollow glass spheres of a specific gravity of 1.4. A high-speed 12 −bit CMOS camera was used to capture instantaneous images of the illuminated particles with a dual-cavity high-speed pulsed Nd:YLF laser. Measurements were performed in three streamwise-spanwise ($x - z$) planes located at $0.5d$ from the bottom wall (P1) to capture the near-wall base vortices, near the mid-height ($y/d = 4.0$) (P2) to capture the von Karman vortex shedding and $0.5d$ from the free end of the DC (P3) to capture the effects of tip vortices for the tandem cylinder. Similar wall-normal locations were used for P1 and P3 of the reference single cylinder, however, P2 was measured at the mid-height ($y/d = 3.5$). The slight upward shift of the P2 for the TC was made to ensure that the plane passes through the induced upwash region behind the DC of the TC. A total sample size of 48000 images was acquired in eight batches of 6000 images/batch at a sampling frequency of $1000\ Hz$. The ratio of the sampling frequency to the spanwise vortex shedding frequency at mid-height of SC was determined as 182 cycles, indicating sufficient temporal resolution to capture the unsteady wake characteristics. Furthermore, the convergence test based on the sample size demonstrated statistical convergence of the turbulence statistics and spectral quantities reported herein. Following Essel et al. [5], the uncertainty in the streamwise mean velocity for the time-resolved measurements at a 95% confidence level ranged from $\pm 1\%$ to $\pm 5\%$ across the cylinder height, while the uncertainties in the Reynolds stresses varied between $\pm 3\%$ to $\pm 14\%$.

III. Results and Discussion

A. Mean Flow and Turbulence Statistics

Fig. 3 shows contours of the spanwise mean velocity in the spanwise planes (P1, P2 and P3) with the mean streamlines superimposed for the SC and TC. In each plot, the reverse flow region ($U < 0$) is demarcated using the contour line of 50% forward fraction flow ($\gamma = 0.5$). A half-section is shown for brevity as the contours are symmetrical at the centerline ($z/d = 0$). The cylinders exhibit a negative spanwise velocity at the fore end due to the flow deflection, whereas entrainment of surrounding fluid is observed behind the cylinders, near the reverse flow region. Behind SC, the entrainment is enhanced near the free end and the base compared to mid-height, which is opposite to the pattern observed in the TC due to shift of saddle point behind UC and DC [10], [11]. The length of the reverse flow region (L_r) determined as the streamwise distance from the rear end surface of the cylinder to the farthest location of the isopleth of 50% forward flow fraction for the SC is largest at P2 ($2.17d$), diminishes at P1 ($1.32d$) and completely suppressed at P3. Behind UC, the length of the reverse flow region increased from $1.55d$ (P2) to $2.51d$ (P1) in contrast to SC which exhibits a decrease in L_r toward the bottom wall. The enhanced region in P1 of the gap region of the TC, compared to that of the SC, is attributed to both wake interference and the stronger upwash behind the SC. In contrast to the SC, behind the DC, the L_r is reduced in the sheltered position of DC (P1 and P2), while the unsheltered portion of the DC exhibits a reverse flow region of $L_r = 0.65d$.

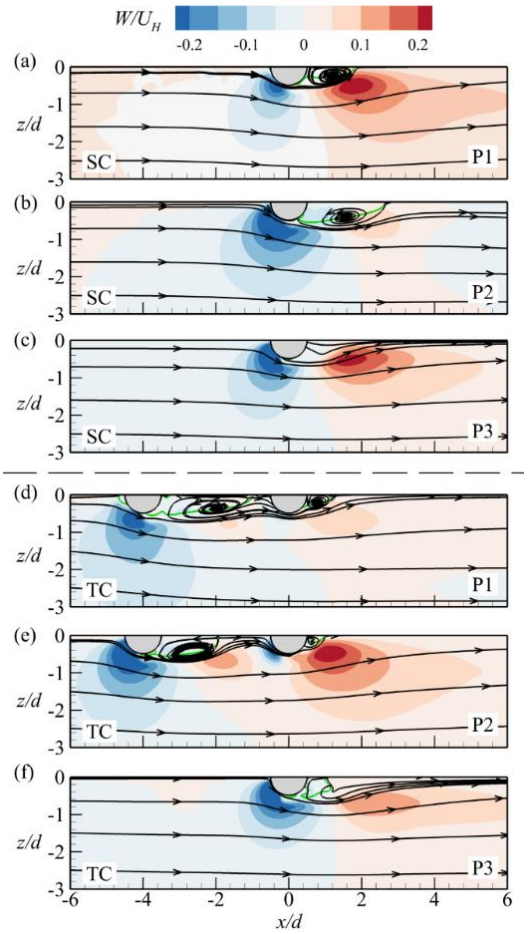

Figure 3. Contours of spanwise mean velocities in the planes, P1, P2 and P3 for SC and TC. Superimposed on the contours are the mean streamlines. The green solid lines represent the isopleth of 50% forward-flow probability which bounds the reverse-flow region.

Contours of streamwise Reynolds normal stresses ($< u'^2 >$) and spanwise Reynolds normal stresses ($< w'^2 >$) are presented in Figs. 4 and 5, respectively. The (×) symbol denotes the location of the local maxima with the magnitude. The $< u'^2 >$ and Reynolds shear stress ($< -uw >$) (contours not shown for brevity) are enhanced in the separated shear layers while $< w'^2 >$ is more intense within the wake behind the cylinder. The higher magnitude of $< w'^2 >$ compared to $< u'^2 >$ showcase a strong anisotropy of the Reynolds stresses in the spanwise plane compared to symmetry plane [5], [10]. The stresses are suppressed near the wall and free ends but enhanced near the mid-height of the cylinders due to the stronger vortex shedding at the mid-height of the cylinders. In contrast to SC, the cylinder ends of DC exhibits more pronounced stress, $< u'^2 >$ near the bottom wall and $< w'^2 >$ and $< -uw >$ near the free end. The effect of wake interference enhanced the Reynolds stresses in front of the DC

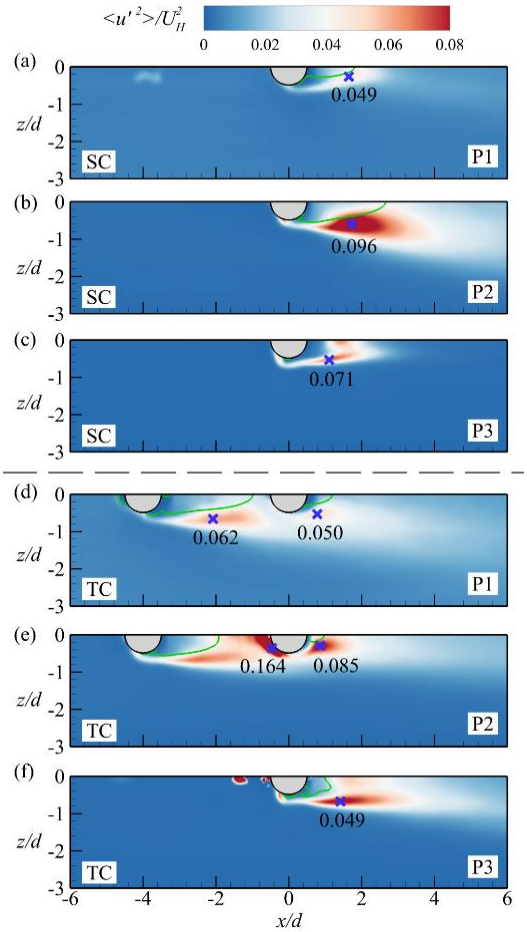

Figure 4. Contours of streamwise Reynolds normal stress in P1, P2 and P3.

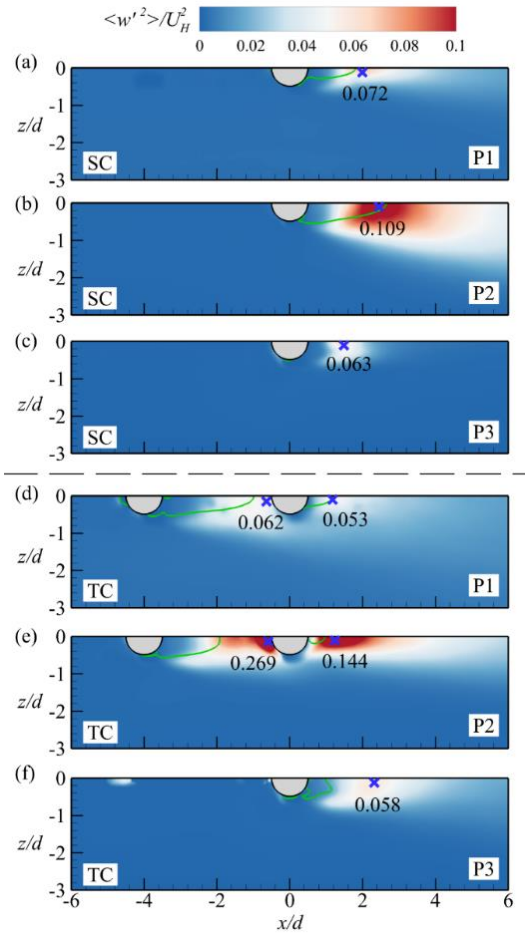

Figure 5. Contours of spanwise Reynolds normal stress in P1, P2 and P3.

and the induced upwash region behind the DC (P2), however the stresses are comparatively lower behind DC compared to SC. As shown in Fig. 5, the location of peak $< w'^2 >$ indicated by blue ($\times$) depicts the intensity of vortex shedding and corresponds to the onset of vortex formation. The farthest occurrence of peak indicates the delay in vortex formation near the unsheltered free end while closer peak shows early formation in the sheltered portion of DC compared to the SC.

B. *Growth of the shear layers*

The growth of the spanwise shear layers is characterized using vorticity thickness defined as

$$\delta_\omega = (\Delta U)/(\partial U/\partial z|_{max}) \qquad (1)$$

where, $\Delta U = U_{max} - U_{min}$, U_{max} and U_{min} are the local maximum and minimum streamwise mean velocities, respectively, and $\partial U/\partial z|_{max}$ is the local maximum mean shear. Figs. 6 and 7 shows the distribution of $\Delta U/U_H$ and δ_ω/d with the origin of the normalized streamwise distance (x^*/d) set at the rear end of each cylinders, respectively. The maximum velocity difference ΔU is enhanced near the cylinder and decays downstream. The mid-height exhibits an enhanced profile for UC and SC compared to the base and free end. In contrast DC, exhibits enhanced ΔU near free end. The vorticity thickness

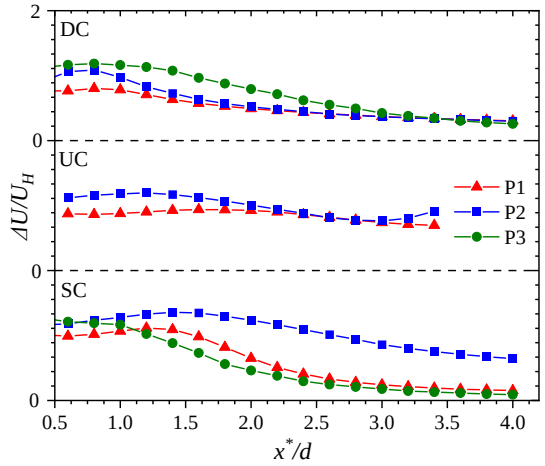

Figure 6. Distributions of velocity difference, $\Delta U/U_\infty$ in the wake region of the FWMCs at the planes, P1, P2 and P3.

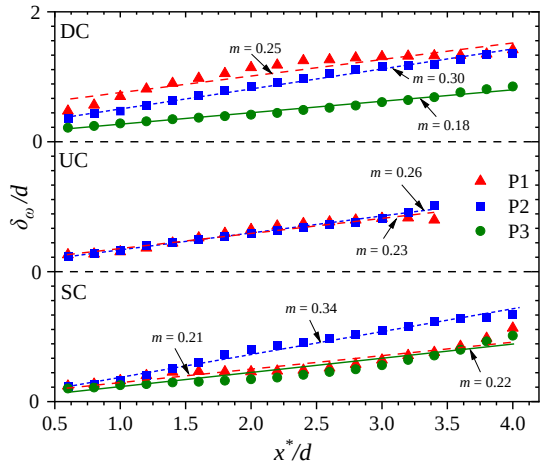

Figure 7. Distributions of vorticity thickness, δ_(ω,y)/d in the wake region of the FWMCs at the planes, P1, P2 and P3.

demonstrates a linear growth rate, $m = d\delta_w/dx^*$ behind each cylinder with larger m at mid-height compared to free end and base. The value of m is 62% larger at the mid-height compared to base for SC, but reduce by 13% for UC and 36% for DC. Near the free end, the growth rate, $m = 0.20 \pm 0.02$ for the SC and the DC is 50% lower compared to the value at the mid-height $m = 0.30 \pm 0.04$. Unlike SC and UC, the growth rate of DC near the free end is lower compared to base, despite larger ΔU at the free end. This observation is attributed rapid decay of mean shear near the free end compared to the base. The present growth rates are within the range $m \in [0.11 - 0.33]$ reported for separated shear layers of forward- and backward-facing steps [12], [13], while $32 - 64\%$ lower than the value ($m = 0.50$) reported for the upwash and downwash separated shear layers of the SC [5].

C. *Spectral Analysis*

The spectra of the streamwise velocity fluctuations are shown by Fig. 8 to investigate the spanwise vortex shedding along the span of each cylinders. The profiles were extracted at the locations of maximum u_{rms} in each plane. For SC, the

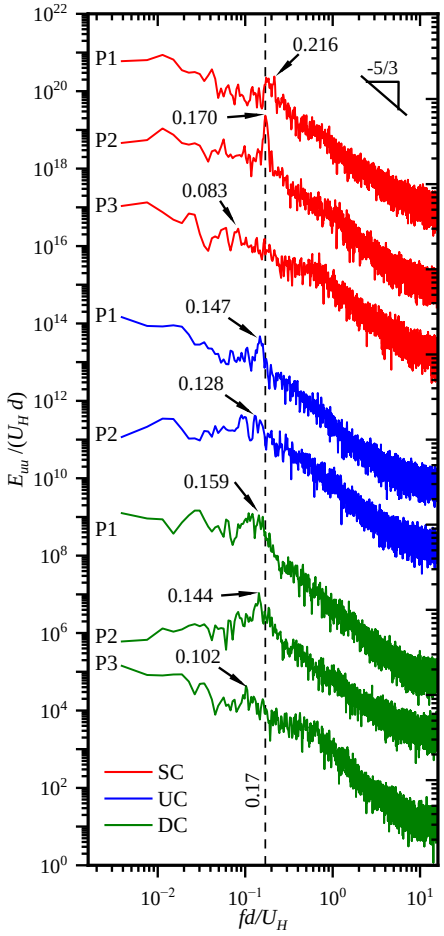

Figure 8. Spectra of the streamwise velocity fluctuations behind the SC, UC and DC for each test case. For clarity, the spectra are offset arbitrarily.

dominant low frequency ($St = 0.083$) near free end, regular shedding frequency ($St = 0.170$) at mid-height and high frequency ($St = 0.216$) near base depict a cellular shedding behavior [5]. Behind the UC of the TC, the dominant vortex shedding frequencies at P1 is $St = 0.147$ and P2 is $St = 0.128$. The vortex shedding frequency behind DC decreases toward the free end ($St = 0.159$ for P1, $St = 0.144$ for P2 and $St = 0.102$ for P3) and are reduced compared to the SC. The frequencies for the spanwise vortex shedding for the TC are lower than values reported for the upwash and downwash shear layers of the UC ($St = 0.249 - 0.283$) and the DC ($St = 0.344$) [11].

D. Spectral Proper Orthogonal Decomposition

The spatial and temporal characteristics of the vortical structures are examined using spectral proper orthogonal decomposition (SPOD). The SPOD method identifies spatially energetic structures of the entire frequency domain and sorts them based on their advection frequencies [14]. In the framework of SPOD, a Fourier transform of the time-resolved flow field is performed, followed by decomposing the Fourier transformed flow field into different mode using the POD technique. The decomposed fluctuating velocity component is expressed as

$$\vartheta'(x,y,t) = \sum_{j=1}^{\infty}\sum_{m=1}^{\infty} \phi_j^m(x,y) a_j^m e^{-i\omega_j t} + c.c. \qquad (2)$$

where ϕ_j^m is the orthogonal set of spatial eigenfunctions (modes) and a_j^m is their corresponding coefficients, and the angular frequencies $\omega_j = 2\pi f_j$. Here the indices j and m represent the frequency and mode number while $i \equiv \sqrt{-1}$ and $c.c.$ denotes the complex conjugate. The SPOD is used to the study of the effects of partial sheltering on the energetic structures associated with vortex shedding in the spanwise planes of the FWMCs. The sample size of 48000 was divided into eight batches, with each batch consisting of 6000 images. Fast Fourier transform (FFT) was performed on each batch using a Hanning window, resulting in a frequency resolution of $\Delta f = 0.12\,Hz$. To optimize computational efficiency, no overlap of batches was set, and the flow field was trimmed to a masked region of $x/d \in [-6,8]$ and $z/d \in [-3,3]$.

The energy spectra of the most dominant mode, Mode 1, is shown in Fig. 9. The spectra of Mode 1 exhibit a dominant Strouhal number of $St = 0.182$ near the free end and base, and $St = 0.174$ at the mid-height of the SC. For the TC, the dominant Strouhal numbers are $St = 0.144, 0.132$ and 0.159 in P1, P2 and P3, respectively. The similar frequency signatures were also observed in the spectra of the velocity fluctuations.

Contours of the spanwise component (ϕ_w) of Mode 1 at the dominant Strouhal number behind each cylinder are presented in Fig. 10. The distance between vertical lines through the peaks of alternating (positive and negative) regions of ϕ_w corresponds to half the local wavelength ($\lambda/2$). Near the wall, the structure shed behind SC exhibits $\lambda \approx 3.5d$. At mid-height, the λ reduced to $2.7d$, attributed to the evolution of larger-scale

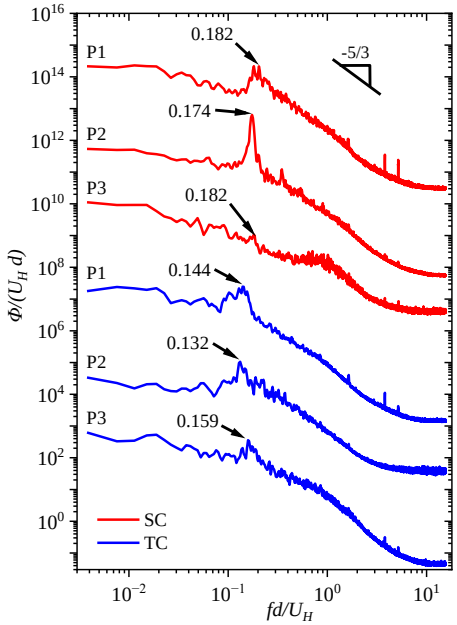

Figure 9. Spectra of SPOD Mode 1 at the dominant Strouhal numbers for SC and TC in the plane P1, P2 and P3.

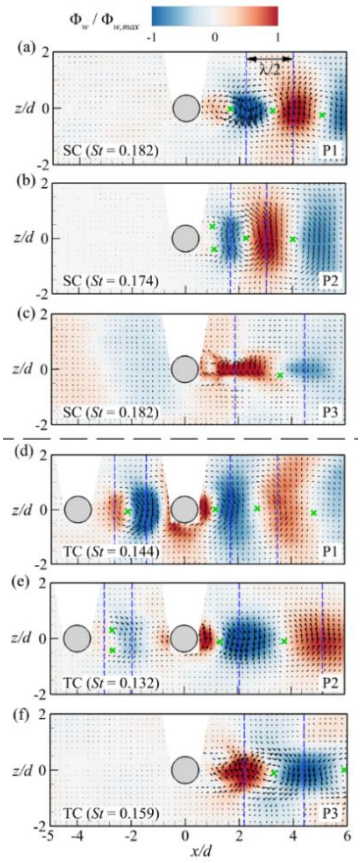

Figure 10. Contours of spanwise (ϕ_w) components of Mode 1 at the dominant Strouhal numbers in P1, P2 and P3 for SC and TC. The vectors of ϕ_u and ϕ_v are shown on each plot.

structures. The structures near the free end are elongated in the streamwise direction and with larger λ of $5.2d$. For the TC, the structures shed from the UC merge with those of the DC, forming larger structures with an enhanced spanwise distribution near the wall compared to the mid-height. Near the wall, the λ of the vortices shed from the UC is $2.4d$ but increased to $3.5d$ downstream of the DC. At P2, the λ for UC is $2.1d$ but increased to $6.2d$ for DC. At P3, the structure has a reduced λ of $4.4d$ compared to those at the mid-height, in agreement with [5].

IV. Conclusion

Time-resolved PIV system was used to investigate the effect of partial sheltering on the spanwise wake characteristics of unequal-height tandem FWMCs. The cylinders of height ratio $h/H = 0.75$ were submerged in a turbulent boundary layer of thickness $\delta/H = 1.2$ for a fixed spacing ratio of $s/d = 4$. Measurements were performed in three streamwise-spanwise planes along the height of the tandem cylinders (TC) and a reference single cylinder (SC).

The wake interference by DC enhanced the flow entrainment from the side in the gap region of the TC which the increased the area of the reverse flow region and reduced the vortex shedding Strouhal number near the wall compared to the SC. Behind DC, the partial sheltering suppressed the reverse flow region in the sheltered portion but enhanced at the unsheltered free end. The reduction in the sheltered portion was influenced by the enhanced entrainment of flow from the side which altered the shedding behavior of the DC by accelerating the onset of vortex formation compared to both the SC and the UC. Furthermore, Reynolds stress were found to be enhanced in front of DC and the induced upwash region behind DC. Frequency spectra of the velocity fluctuations and SPOD analysis showed that the Strouhal number of the spanwise vortex shedding of DC is lower at mid-height characterized by larger vortices and larger wavelength compared to near the base and free end. This observation was in contrast to SC.

Acknowledgment

The authors are grateful to the Natural Sciences and Engineering Research Council of Canada (NSERC) for their financial support through a Discovery Grant for E.E.E. We are also grateful to Canada Foundation for Innovation (CFI) for funding for the experimental facility at the University of Manitoba.

References

[1] A. M. Hamed, A. M. Peterlein, and L. V. Randle, "Turbulent boundary layer perturbation by two wall-mounted cylindrical roughness elements arranged in tandem: Effects of spacing and height ratio," *Phys. Fluids*, vol. 31, no. 6, Jun. 2019.

[2] M. M. Zdravkovich, *Flow Around Circular Cylinders: Volume 2: Applications*, vol. 2. Oxford, U.K.: Oxford University Press, 1997.

[3] D. Sumner, J. L. Heseltine, and O. J. P. Dansereau, "Wake structure of a finite circular cylinder of small aspect ratio," *Exp. Fluids*, vol. 37, no. 5, pp. 720–730, Nov. 2004.

[4] R. J. Pattenden, S. R. Turnock, and X. Zhang, "Measurements of the flow over a low-aspect-ratio cylinder mounted on a ground plane," *Exp. Fluids*, vol. 39, no. 1, pp. 10–21, Jul. 2005.

[5] E. E. Essel, M. F. Tachie, and R. Balachandar, "Time-resolved wake dynamics of finite wall-mounted circular cylinders submerged in a turbulent boundary layer," *J. Fluid Mech.*, vol. 917, 2021.

[6] D. Sumner and H. K. Reitenbach, "Wake interference effects for two finite cylinders: A brief review and some new measurements," *J. Fluids Struct.*, vol. 89, pp. 25–38, Aug. 2019.

[7] S. Krajnović, "Flow around a tall finite cylinder explored by large eddy simulation," *J. Fluid Mech.*, vol. 676, pp. 294–317, Jun. 2011.

[8] D. Sumner and H. Li, "Wake interference effects for two surface-mounted finite cylinders in a tandem configuration," in Pressure Vessels and Piping Conference, vol. 46018, p. V004T04A007, Jul. 2014, American Society of Mechanical Engineers.

[9] Y. Zhou and M. W. Yiu, "Flow structure, momentum and heat transport in a two-tandem-cylinder wake," *J. Fluid Mech.*, vol. 548, no. 1, p. 17, Feb. 2006.

[10] E. E. Essel, R. Balachandar, and M. F. Tachie, "Effects of sheltering on the unsteady wake dynamics of tandem cylinders mounted in a turbulent boundary layer," *J. Fluid Mech.*, vol. 954, Jan. 2023.

[11] N. F. Ouedraogo and E. E. Essel, "Unsteady wake interference of unequal-height tandem cylinders mounted in a turbulent boundary layer," *J. Fluid Mech.*, vol. 977, Dec. 2023.

[12] E. E. Essel and M. F. Tachie, "Roughness effects on turbulent flow downstream of a backward facing step," *Flow Turbul. Combust.*, vol. 94, no. 1, pp. 125–153, Jan. 2015.

[13] X. Fang and M. F. Tachie, "On the unsteady characteristics of turbulent separations over a forward-backward-facing step," *J. Fluid Mech.*, vol. 863, pp. 994–1030, Mar. 2019.

[14] A. Towne, O. T. Schmidt, and T. Colonius, "Spectral proper orthogonal decomposition and its relationship to dynamic mode decomposition and resolvent analysis," *J. Fluid Mech.*, vol. 847, pp. 821–867, Jul. 2018.